

# Fluorescence tomography with the frequency domain equation of radiative transfer

Alexander D. Klose †, Hyun K. Kim††, and  
Andreas H. Hielscher †, ††

†Dept. of Radiology, Columbia University  
MC 8904, 500 West 120th Street, New York, NY 10027, USA  
Email: ak2083@columbia.edu

††Dept. of Biomedical Engineering, Columbia University  
MC 8904, 500 West 120th Street, New York, NY 10027, USA

## Abstract:

We have developed an image reconstruction algorithm for fluorescence tomography based on the frequency domain equation of radiative transfer. Transport properties of tissue become significant when strong light absorption is encountered at visible wavelengths of light propagation in tissue with small geometries.

© 2007 Optical Society of America

OCIS codes: (170.3660) light propagation in tissue, (170.6960) tomography.

## 1 Introduction

Considerable progress has been made in recent years towards optical tomographic imaging of fluorescent markers in biological tissues. This progress has already resulted in several commercial small animal imaging systems. [1] However, a major problem remains that all these system rely on the diffusion approximation in the tomographic imaging process. The diffusion approximation to the equation of radiative transfer (ERT) is already widely applied for modeling light propagation in tissue with relatively large geometries, such as brain and breast tissue [1]. However, when imaging small tissue geometries, e.g. small animals, the diffusion model becomes less accurate, partly because boundary effects become significant. Also, when using visible instead of near-infrared light, as it is done in fluorescence imaging of green fluorescent proteins (GFP), high tissue absorption is encountered. In those cases the diffusion model is not a good approximation to the ERT [2]. Thus, higher-order approximations to the ERT are required, such as the discrete-ordinates ( $S_N$ ), spherical harmonics ( $P_N$ ), or the simplified spherical harmonics ( $SP_N$ ) approximation. [3, 4]

GFP is now used in many biological and medical applications. For example, more animal models for cancer development (oncogenesis) and cancer progression (metastasis) have become available and optical surface imaging has successfully been applied. However, GFP imaging in deep tissue of small animals remains problematic due to the strong absorption of light in the visible spectrum (wavelengths  $< 550$  nm), and due to strong background signals caused by tissue autofluorescence.

## 2 Frequency-domain equation of radiative transfer

Fluorescence light propagation in scattering tissue can be described by a set of two ERTs [5, 6]. The first equation describes the propagation of excitation light, originating from a boundary source, to the fluorescent source inside tissue. The fluorescent source, i.e. the fluorescent protein, partially absorbs the excitation light and, in turn, emits fluorescence light. The absorption coefficient,  $\mu_a^{x \rightarrow m}$ , of the excitation light is proportional to the concentration and extinction coefficient of the fluorescent source. Furthermore, the amount of light that is emitted by the source is proportional to its absorption coefficient and the quantum yield,  $\eta$ . In the presence of an intensity-modulated excitation light source with modulation frequency  $\omega$ , the emitted fluorescence light will be phase-shifted with respect to the excitation light. The phase shift is caused by the average lifetime,  $\tau$ , of the excited state of the fluorescence source.

The frequency-domain ERT at the excitation wavelength is given for the radiance  $\psi^x(\mathbf{r}, \boldsymbol{\Omega}, \omega)$  at spatial position  $\mathbf{r}$  and direction  $\boldsymbol{\Omega}$ :

$$\left( \boldsymbol{\Omega} \cdot \nabla + \mu_a(\mathbf{r}) + \mu_a^{x \rightarrow m}(\mathbf{r}) + \mu_s(\mathbf{r}) + \frac{i\omega}{v} \right) \psi^x(\mathbf{r}, \boldsymbol{\Omega}, \omega) = \mu_s(\mathbf{r}) \int_{4\pi} p(\boldsymbol{\Omega} \cdot \boldsymbol{\Omega}') \psi^x(\mathbf{r}, \boldsymbol{\Omega}', \omega) d\Omega' . \quad (1)$$

The absorption,  $\mu_a$ , and scattering,  $\mu_s$ , coefficients describe the intrinsic tissue properties. The absorption coefficient of the fluorescent source is given by  $\mu_a^{x \rightarrow m}(\mathbf{r})$ . We also consider partial reflective boundary conditions and boundary sources  $S(\mathbf{r}, \boldsymbol{\Omega}, \omega)$  with  $\psi(\mathbf{r}, \boldsymbol{\Omega}, \omega) = S(\mathbf{r}, \boldsymbol{\Omega}, \omega) + R(|\boldsymbol{\Omega}' \cdot \mathbf{r}|) \psi(\mathbf{r}, \boldsymbol{\Omega}', \omega)$  for all  $\mathbf{n} \cdot \boldsymbol{\Omega} < 0$  at  $\partial V$  with  $\mathbf{n}$  as normal vector on the tissue surface.  $R$  constitutes the reflectivity as determined by *Fresnel's* law. The source  $S(\mathbf{r}, \boldsymbol{\Omega}, \omega)$  at the tissue boundary is given by  $S_0(\mathbf{r}, \boldsymbol{\Omega}) e^{i\omega t}$  for the modulation frequency  $\omega$  and maximum source power density  $S_0(\mathbf{r}, \boldsymbol{\Omega})$ .

The frequency-domain ERT for the fluorescence light has no external source  $S(\mathbf{r}, \boldsymbol{\Omega}, \omega) = 0$ , but an interior fluorescent source that is intensity-modulated by the excitation field  $\phi^x(\mathbf{r}, \omega)$  derived from equation 1. Hence, we obtain

$$\left( \boldsymbol{\Omega} \cdot \nabla + \mu_a(\mathbf{r}) + \mu_s(\mathbf{r}) + \frac{i\omega}{v} \right) \psi^m(\mathbf{r}, \boldsymbol{\Omega}, \omega) = \mu_s(\mathbf{r}) \int_{4\pi} p(\boldsymbol{\Omega} \cdot \boldsymbol{\Omega}') \psi^m(\mathbf{r}, \boldsymbol{\Omega}', \omega) d\Omega' + \frac{1}{4\pi} \frac{\eta \mu_a^{x \rightarrow m} \phi^x}{1 - i\omega\tau} . \quad (2)$$

The partial boundary flux for the fluorescence light is obtained for all detector positions  $\mathbf{r}_d$

$$J^+(\mathbf{r}, \omega) = \int_{\boldsymbol{\Omega} \cdot \mathbf{n} > 0} [1 - R(\boldsymbol{\Omega} \cdot \mathbf{n})] (\boldsymbol{\Omega} \cdot \mathbf{n}) \psi^m(\mathbf{r}, \boldsymbol{\Omega}, \omega) d\Omega . \quad (3)$$

with  $\mathbf{n}$  being the outer normal vector of the tissue boundary, and  $R$  being the reflectivity.

The ERTs can be solved with a finite-difference discrete-ordinates ( $S_N$ ) method [5].

### 3 Solution technique

Both ERTs, equations (1) and (2), are solved numerically by discretizing the spatial variable  $\mathbf{r}$  on a *Cartesian* grid. The spatial derivative is replaced by a finite-difference approximation, called *diamond scheme*. The diamond scheme does not require a fine grid as the step method that has previously been applied in fluorescence tomography [5]. Therefore, the ERT is solved for considerably less grid points, hence, improving the computational speed. The angular variable  $\boldsymbol{\Omega}$  is replaced with discrete ordinates  $\boldsymbol{\Omega}_k$ . Finally, the resulting algebraic system of equations is solved with a source iteration method.

The diamond scheme yields the following expression at grid point  $(i, j)$  on a two-dimensional grid and ordinates  $\boldsymbol{\Omega}_k$  ( $\xi_k > 0$ ,  $\eta_k > 0$ ) for the source iteration method:

$$\psi_{ijk}^{n+1} = \frac{\frac{1}{4\pi} \frac{\eta [\mu_a^{x \rightarrow m}]_{ij} \phi_{ij}^x}{1 - i\omega\tau} + [\mu_s]_{ij} \sum_{k'} w_{k'} p_{kk'} \psi_{ijk'}^n + 2 \frac{\xi_k}{\Delta x} \psi_{i-\frac{1}{2}jk}^{n+1} + 2 \frac{\eta_k}{\Delta y} \psi_{ij-\frac{1}{2}k}^{n+1}}{2 \frac{\xi_k}{\Delta x} + 2 \frac{\eta_k}{\Delta y} + [\mu_a]_{ijl} + [\mu_s]_{ijl} + \frac{i\omega}{v}} , \quad (4)$$

and with auxiliary equations:

$$\psi_{i+\frac{1}{2}jk}^{n+1} = 2\psi_{ijk}^{n+1} - \psi_{i-\frac{1}{2}jk}^{n+1} \quad (5)$$

$$\psi_{ij+\frac{1}{2}k}^{n+1} = 2\psi_{ijk}^{n+1} - \psi_{ij-\frac{1}{2}k}^{n+1} . \quad (6)$$

#### 4 Image reconstruction

The spatial distribution of the fluorescent source absorption coefficient,  $\mu_a^{x \rightarrow m}(\mathbf{r})$ , is reconstructed by minimizing an objective function  $\Phi(\mu_a^{x \rightarrow m})$  with a Broyden-Fletcher-Goldfarb-Shanno (BFGS) method [5]. The objective function describes the difference between the measured,  $Y^m$ , and predicted data,  $J_d^m$ , for all D source-detector pairs

$$\Phi(\mu_a^{x \rightarrow m}) \approx \sum_{d=1}^D \left( \frac{J_d^m - Y_d^m}{\sigma} \right)^2. \quad (7)$$

The predicted detector readings at the emission wavelength,  $\lambda^m$  of the fluorescent source, are calculated by Equation (2), whereas the excitation field at  $\lambda^x$  is determined by Equation (1). Both quantities,  $Y$  and  $J^+$ , contain the amplitude and phase information.

As a first example Fig. 1 shows a numerical reconstruction result for a modulation frequency of 100 Mhz. The numerical model (size: 2 cm x 2 cm) consisted of  $\mu_s = 10 \text{ cm}^{-1}$  and  $\mu_a = 1 \text{ cm}^{-1}$ . The code recovers the position as well as the concentration of two single fluorescent sources. More extensive studies that elucidate the advantages of frequency-domain transport code for fluorescence imaging are under way.

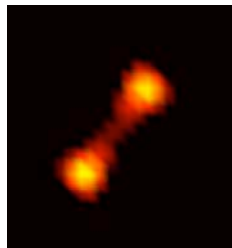


Fig. 1. Image reconstruction of fluorophore absorption of two single targets with diameter of 3 mm.

This work is supported in part by a grant (1R21CA118666-01A2) from the National Institutes of Health (NIH).

#### References

1. A.P. Gibson, J.C. Hebden, S.R. Arridge, "Recent advances in diffuse optical imaging," *Phys. Med. Biol.* 50, R1-R43 (2005).
2. A.H. Hielscher, R.E. Alcouffe, and R.L. Barbour, "Comparison of finite-difference transport and diffusion calculations for photon migration in homogeneous and heterogeneous tissues," *Phys. Med. Biol.* 43, 1285 (1998).
3. K.M. Case and P.F. Zweifel, *Linear Transport Theory*, Addison Wesley, Reading, 1967.
4. A.D. Klose and E.W. Larsen, "Light transport in biological tissue based on the simplified spherical harmonics equations," *J. Comp. Phys* 220, 441-470 (2006).
5. A.D. Klose, V. Ntziachristos, and A.H. Hielscher, "The inverse source problem based on the radiative transfer equation in optical molecular imaging," *J. Comp. Phys* 202, 323-345 (2005).
6. J. Chang, H.L. Graber, and R.L. Barbour, "Imaging of fluorescence in highly scattering media," *IEEE Transactions on Biomedical Engineering* 44(9), 810 (1997).